

Probabilistic Monte Carlo Based Mapping of Cerebral Connections Utilising Whole-Brain Crossing Fibre Information

Geoff J.M. Parker¹ and Daniel C. Alexander²

¹ Imaging Science & Biomedical Engineering,
University of Manchester, Manchester M13 9PT, UK

geoff.parker@man.ac.uk,
<http://www.man.ac.uk/~gjp>

² Department of Computer Science,
University College London, Gower Street, London WC, UK
d.alexander@cs.ucl.ac.uk

Abstract. A methodology is presented for estimation of a probability density function of cerebral fibre orientations when one or two fibres are present in a voxel. All data are acquired on a clinical MR scanner, using widely available acquisition techniques. The method models measurements of water diffusion in a single fibre by a Gaussian density function and in multiple fibres by a mixture of Gaussian densities. The effects of noise on complex MR diffusion weighted data are explicitly simulated and parameterised. This information is used for standard and Monte Carlo streamline methods. Deterministic and probabilistic maps of anatomical voxel scale connectivity between brain regions are generated.

1 Introduction

Probabilistic methods for determining the connectivity between brain regions using information obtained from diffusion MRI have recently been introduced [3,8,9,10,11,15]. These approaches utilise probability density functions (PDFs) defined at each point within the brain to describe the local uncertainty in fibre orientation. Each PDF is intended to interpret the information available from a diffusion imaging acquisition in terms of the likely underlying fibre structure. Given an accurate voxelwise PDF it should be possible to define the probability of anatomical connection, defined at the voxel scale, between any two points within the brain. This may be achieved using Monte Carlo approaches based on, for example, streamlines [9,10,11] or Bayesian methods [3,15].

To date, PDFs used in probabilistic connectivity methods have either been defined in terms of the diffusion tensor model [3,8,9,10,11] or using q-space approximations acquired from spatially undersampled brain data [15]. The single tensor model of diffusion assumes that diffusive water molecule displacements are Gaussian distributed, which is a poor approximation where fibres cross, diverge, or experience high curvature. This leads to either inaccurate PDFs, which may

assign unwarranted confidence in fibre orientation, or overly conservative PDFs that reflect the ambiguous fibre orientation information provided by the tensor in these regions. The signal to noise ratio (SNR) and sampling requirements of q-space based approaches such as diffusion spectrum imaging [15] make it impractical to perform whole brain imaging at the resolution required for diffusion-based connectivity mapping. At best, only low resolution imaging or restricted volume acquisitions are possible, both of which are obstacles to inter-regional connectivity mapping.

An additional drawback of many suggested PDFs is their somewhat obscure meaning in terms of the phenomena that they are attempting to describe. Examples include the PDFs proposed by Parker *et al*, Lazar & Alexander, and Koch *et al*, each of which is a heuristic attempt to interpret tissue microstructural arrangement from the parameters of the estimated diffusion tensor [8,9,10,11], without providing much justification. The diffusion spectrum PDFs proposed by Tuch *et al* describe the probability of a structural obstruction to diffusion being oriented along one or more directions [15]. However, even a PDF such as this, which has a theoretically close relationship with the underlying structure, does not take into account the influence of data noise on the confidence that may be assigned to an estimated fibre direction.

A promising approach for identifying voxels containing crossing fibres using spherical harmonic fits to diffusion orientation profiles has recently been described [5,2]. These techniques use whole brain multi-directional diffusion encoded data originally designed to allow enhanced SNR diffusion tensor imaging on standard clinical scanners [6]. These data are not suitable for invoking standard q-space-based methods but can reveal locations in the brain where the single tensor model is poor, indicating fibre crossings [5,2]. These datasets have the advantages of being acquired on clinical scanners, thus allowing access to patient cohorts, and higher spatial resolution and coverage than acquisitions designed for q-space imaging. For this work, we assume that voxels in which the single tensor fits the data poorly are fibre crossings and we fit a multi-Gaussian model instead. We simulate the effect of data noise on these fits, allowing us to generate noise-based PDFs in regions containing crossings. Uncertainty in single fibre voxels is parameterised in the same way with the aid of a single Gaussian model. This set of methods represents a promising approach for performing whole-brain, high resolution, probabilistic connectivity mapping to defined seed points that accounts for crossing fibre tracts.

2 Methods

2.1 Data Acquisition

Single-shot echo planar diffusion weighted brain data were acquired using a GE Signa 1.5 tesla scanner with a standard quadrature head coil. Sequence parameters: cardiac gating (TR = 20 RR \approx 20 s); 60 axial slices; TE = 95 ms; 54 non-collinear diffusion-weighting directions at $b = 1156 \text{ smm}^{-2}$ (calculated according to [13]); 6 acquisitions with a $b \sim 0 \text{ smm}^{-2}$; diffusion sensitisation

gradient duration $\delta = 34$ ms; interval between gradients $\Delta = 40$ ms; gradient strength $G = 22$ mTm⁻¹; 96×96 acquisition matrix, interpolated during reconstruction to 128×128 ; 220 mm field of view, generating $2.30 \times 2.30 \times 2.30$ mm³ voxels as acquired, which are reconstructed to $1.72 \times 1.72 \times 2.30$ mm³ [6, 16]. The total acquisition time was approximately 20 minutes. Eddy current induced image distortions in the diffusion sensitised images were removed using affine multiscale two-dimensional registration [14]. The brain was extracted on the $b = 0$ images to provide a brain mask using the brain extraction tool (BET) available in the FSL software package (<http://www.fmrib.ox.ac.uk>).

All subjects were scanned with ethical committee approval and gave informed, written consent. The SNR of the data was defined as the mean $b = 0$ signal divided by the mean standard deviation of signal in a range of uniform tissue regions. For the data used in this study a SNR value of 16 was obtained.

2.2 Voxel Classification

We use the algorithm of Alexander *et al* [2] to identify voxels in which the single tensor model is poor. In these voxels we fit a mixture of two Gaussian densities; otherwise we use the single tensor model. The principal diffusion directions (PDDs) of the two diffusion tensors in the mixture model provide estimates of the orientations of the crossing fibres.

We define

$$d(\hat{\mathbf{k}}) = b^{-1} \left(\log S(\hat{\mathbf{k}}, b) - \log S(\hat{\mathbf{k}}, 0) \right), \quad (1)$$

where $S(\hat{\mathbf{k}}, b)$ is the MRI measurement with diffusion weighting gradient direction $\hat{\mathbf{k}}$ and diffusion weighting factor b . For the single tensor model

$$d(\hat{\mathbf{k}}) = \hat{\mathbf{k}}^T \mathbf{D} \hat{\mathbf{k}}. \quad (2)$$

This model provides a suitable description of diffusion in tissues where a single fibre bundle direction is present in an image voxel. In voxels containing n different fibre directions a multi-Gaussian model [1,5] can be more appropriate:

$$S(\hat{\mathbf{k}}, b) = S(0) \sum_{i=1}^n a_i \exp \left[-b \hat{\mathbf{k}}^T \mathbf{D}_i \hat{\mathbf{k}} \right]. \quad (3)$$

As described in [2], we use a spherical harmonic model of $d(\hat{\mathbf{k}})$ to identify voxels in which the single tensor model is poor. Thus

$$d(\hat{\mathbf{k}}) = \sum_{l=0}^{\infty} \sum_{m=-l}^l c_{lm} Y_{lm}(\hat{\mathbf{k}}), \quad (4)$$

where Y_{lm} is the spherical harmonic of order l and index m . Since $d(\hat{\mathbf{k}})$ is real and $d(\hat{\mathbf{k}}) = d(-\hat{\mathbf{k}})$, $c_{lm} = 0$ when l is odd and $c_{lm} = (-1)^m c_{l-m}^*$. We truncate the series at order 0, 2 or 4 using the analysis of variance test for deletion of variables

to select the best model. When the series is truncated at order 0, diffusion is isotropic. When it is truncated at order 2, the single tensor model is a good approximation and Eqs. 2 and 4 are equivalent. When fourth-order terms are included in the series, the single tensor fit is poor and we fit the multi-Gaussian model with $n = 2$. We assume that we cannot resolve the directions of more than two fibres with the number (54) of diffusion-weighted measurements acquired.

To fit the multi-Gaussian model, we use a Levenberg–Marquardt algorithm on data resampled from the spherical harmonic model of $d(\mathbf{k})$. Figure 1 shows a region of the brain demonstrating crossing fibre content. This region, where the motor tract (a superior-inferior tract) crosses the superior longitudinal fasciculus (an anterior-posterior tract at this position) and fibres from the corpus callosum are passing left-right, demonstrates the widespread presence of fibre crossings and their potential impact on the directional information present within the brain. Figure 1 also demonstrates the ease with which regions containing crossing fibres may be overlooked in conventional diffusion tensor imaging.

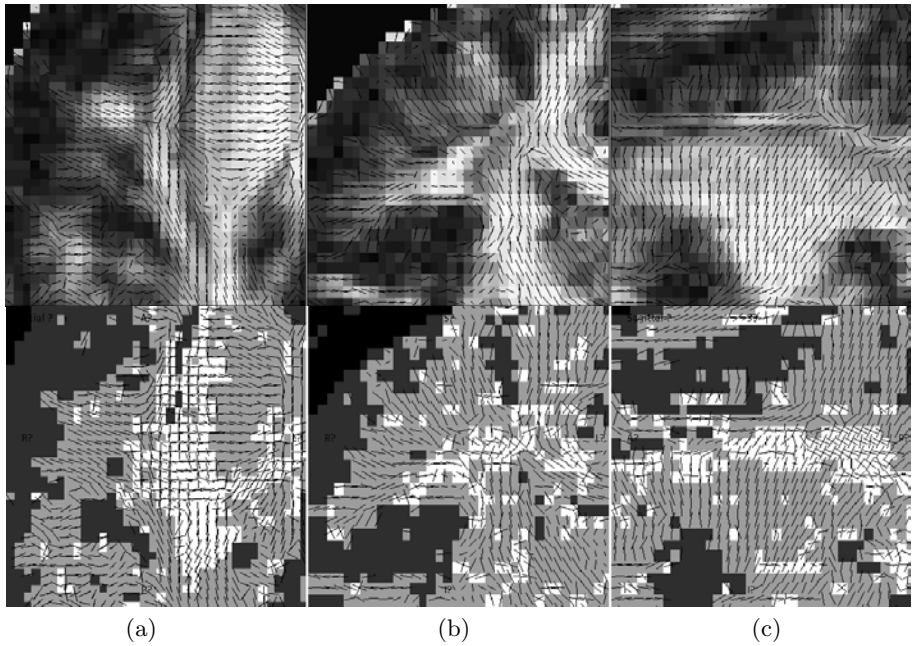


Fig. 1. Comparison of single tensor (top) and biGaussian modelling (bottom). Top: Greyscale linearly proportional to tensor fractional anisotropy (FA) [12]. Bottom: Voxels containing single, isotropic tensors (dark grey), single anisotropic tensors (mid-grey), and two tensors (white). Region shown is in the vicinity of the right corona radiata. Black needles represent PDDs. Note that low FA values outside grey matter in the single tensor parameterisation (top) often correspond to regions of crossing fibres (bottom). However, even relatively high anisotropy regions may demonstrate crossing fibres. (a) axial; (b) coronal; (c) sagittal views

2.3 Noise-Based Uncertainty in Principal Diffusion Direction

The effect of noise on the single or two tensor fitting process is modelled using a simulated complex MR measurement. We add zero-mean random Gaussian-distributed noise with $\text{SNR} = 16$ repeatedly to estimate the PDF describing the effects of noise on apparent fibre direction.

Noise model. We define a PDF in the PDD by simulating the addition of noise to complex MR data. The mean brain $b = 0$ signal (S_0), δ , Δ , the data noise level, and the b -matrix are used as simulation inputs. We fit the spherical harmonic series to the simulated noisy data followed by the multi-Gaussian model. For a given δ , Δ , and S_0 , the degree of deviation of the PDD about its expected direction is dependent upon the noise level, and the relative and absolute magnitudes of the tensor eigenvalues, $\lambda_1, \lambda_2, \lambda_3$ (table 1). Within the simulation we constrain the range of $\lambda_1, \lambda_2, \lambda_3$ by using the fact that the trace of the diffusion tensor varies little in brain tissue. We reduce the simulation set by assuming that $\lambda_2 = \lambda_3$ (i.e. that we only encounter axially symmetric tensors). In voxels exhibiting partial volume effects (for example in the presence of crossing fibres) non-axially symmetric tensors may be expected; however as we are explicitly detecting and modelling these cases it is likely to be a good assumption that all remaining single tensors are indeed axially symmetric. By extension we also assume that cases with two non-axially symmetric tensors do not occur.

Table 1. Eigenvalues and fractional anisotropy, FA [12], used in the noise simulation. A constant value of trace = $2100 \times 10^{-6} \text{mm}^2 \text{s}^{-1}$ was used for all experiments

FA	0.1	0.2	0.3	0.4	0.5	0.6	0.7	0.8	0.9
λ_1 ($\times 10^{-6} \text{mm}^2 \text{s}^{-1}$)	781	864	950	1042	1143	1256	1390	1554	1773
λ_2, λ_3 ($\times 10^{-6} \text{mm}^2 \text{s}^{-1}$)	660	618	575	529	479	422	355	273	164

Single fibre case. For the single axially-symmetric tensor model, the addition of Gaussian noise generates PDD distributions as shown in Fig. 2. If we align the z axis along the original PDD, the PDF is independent of longitudinal angle, ϕ , and has approximately normally distributed dependence on angle of deflection, θ , with a mean coincident with the original PDD ($\theta \in [-\pi/2, \pi/2]$, $\phi \in [-\pi/2, \pi/2]$). Figure 3 shows the standard deviation in θ as a function of FA . This is in line with the results of [7], but clarifies the dependence of the PDD on noise in the axially symmetric limit. The deviations of the fitted lines in Fig. 3 from the data points may be due to the choice of a normal model of θ . It is possible that the use of a dedicated spherical distribution such as a von Mises - Fisher distribution may improve the parameterisation at low FA .

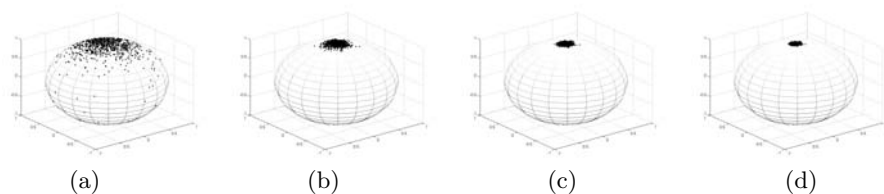


Fig. 2. Simulated distribution of PDD due to random Gaussian distributed noise as a function of FA . Noiseless orientation of PDD along vertical (z) axis. Axial symmetry of tensor assumed. (a) $FA = 0.1$; (b) $FA = 0.3$; (c) $FA = 0.5$; (d) $FA = 0.7$

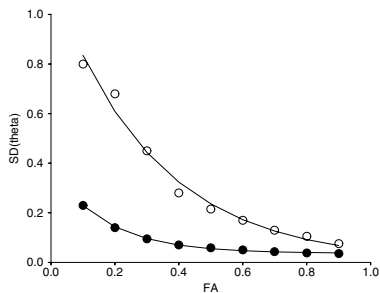


Fig. 3. Standard deviation (σ_θ) in θ , due to the addition of Gaussian noise at $SNR = 16$ as a function of FA . The relationship between σ_θ and tensor FA is well described by a biexponential function, allowing uncertainty in θ to be estimated from the anisotropy of the fitted tensor. Closed circles: σ_θ of PDD of single tensor (no crossing fibres present). Open circles: σ_θ of PDD of one of two tensors when crossing fibres are present

Two fibre case. For the mixture model two PDDs exist, representing the axes of two crossing fibres. Examples of the distribution of these directions under the addition of Gaussian noise to the simulated complex MR data are shown in Fig. 4. The mean orientation of each fibre is not greatly affected by the presence of the neighbouring fibre. Furthermore, the spread in orientation of each is affected little by the relative orientation or spread of the other. With this observation we assume that the distributions of fitted PDDs for each fibre may be treated independently. As in the single fibre case, we use a Gaussian model for the distribution of the angle of deflection, the parameters of which are a function of FA for each tensor. As can be seen in Fig. 3, the uncertainty associated with the PDD of a tensor when crossing fibres are present is larger than that in the single fibre case, due to the larger set of fitted parameters.

2.4 Streamline Propagation in the Multi-tensor Field

A step in the streamline propagation process is defined:

$$\mathbf{X}(l+1) = \mathbf{X}(l) + \mathbf{w}(l)\delta t, \quad (5)$$

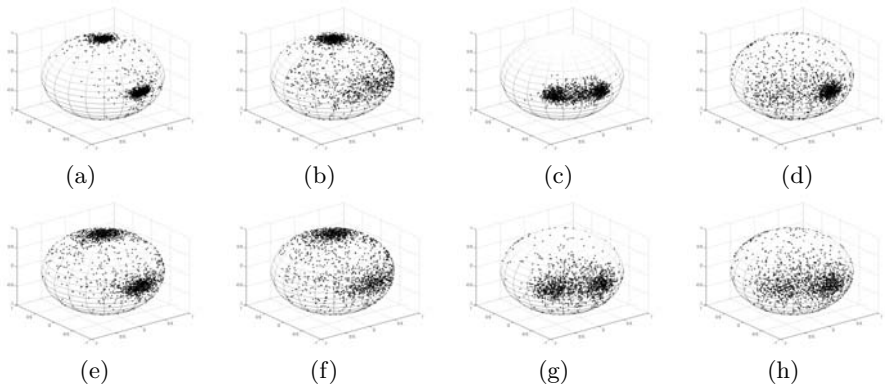


Fig. 4. Simulated distribution of fitted PDDs due to random Gaussian distributed noise for a range of crossing fibre cases. Axial symmetry of both tensors is assumed and fibres are present in equal proportions. Noiseless fibre orientation: (a,b,e,f) y, z ; (c,d,g,h) xy, y . FA values for each tensor: (a) 0.9, 0.9; (b) 0.3, 0.9; (c) 0.9, 0.9; (d) 0.3, 0.9; (e) 0.7, 0.7; (f) 0.5, 0.7; (g) 0.7, 0.7; (h) 0.5, 0.7

where $\mathbf{X}(l)$ is the position in \mathbb{R}^3 of the streamline at point l on its length, $\mathbf{w}(l)$ is the propagation direction at this point ($l \mapsto \mathbf{X}$), and δt is the step size. With a single tensor model of diffusion, $\mathbf{w}(l)$ is defined as the interpolated PDD at that point. We achieve this by trilinear interpolation of surrounding tensor elements to provide an interpolated tensor, from which the local PDD is determined. In the case where one or more of the image voxels involved in the interpolation is described by more than one tensor we employ selection rules to ensure the most appropriate tensor is included in the interpolation. If $\mathbf{D}_i(\mathbf{p})$ is one of n tensors present at image location \mathbf{p} , a location to be included in the interpolation, then the selected tensor is that which satisfies

$$\max_i (|\Gamma(\mathbf{D}_i(\mathbf{p})) \cdot \mathbf{w}(l-1)|) , \tag{6}$$

where $\Gamma(\mathbf{D}_i(\mathbf{p}))$ is the PDD of the i^{th} tensor at \mathbf{p} . This formulation ensures that when fibre crossing is detected, the tensor representing the fibre with an orientation closest to that of the current streamline propagation direction is chosen to influence further propagation. Figure 5(a) demonstrates the propagation of streamlines through a region of crossing fibres.

2.5 Monte Carlo Methods and Maps of Connection Probability

The PICo framework is used to enable probabilistic fibre tracking [10,11], allowing maps of connection probability to be generated. The method utilises a Monte Carlo streamline approach, sampling the orientation PDFs within each voxel on each iteration. Fig. 5(b) illustrates the deviation of streamlines due to the cumulative effects of PDFs within each imaging voxel.

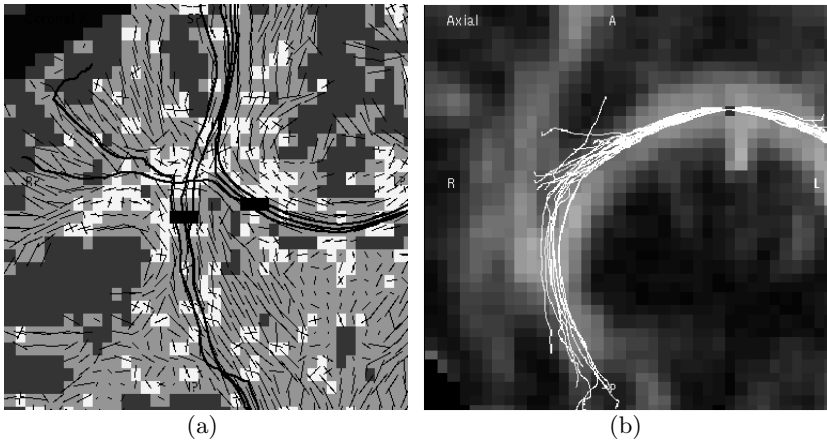


Fig. 5. (a) Streamline propagation through a region of crossing fibres in the vicinity of the example in Fig. 1. Streamlines (black continuous lines) initiated in the corpus callosum propagate left-right through the regions, whilst initiation in the corticospinal tract leads to inferior-superior propagation. (b) Illustration of streamline randomisation process in the corpus callosum

The number of occasions, $\mu(\mathbf{p}, N)$, over N repetitions at which each voxel, \mathbf{p} , is crossed by a streamline is used to define a map of the probability, ψ , of connection to the start point, in a similar fashion to [8]:

$$\psi(\mathbf{p}) = \lim_{N \rightarrow \infty} \frac{\mu(\mathbf{p}, N)}{N} \approx \frac{\mu(\mathbf{p}, N)}{N}. \quad (7)$$

3 Probabilistic Fibre Tracking Examples

A number of examples from a single subject are presented. Figure 6 shows maps of connection probability to a single voxel in the middle of the splenium of the corpus callosum. Branching of the extracted pathway may be observed at various points, with a branch of relatively high probability in the left hemisphere. However, the main route of connection is tightly localised between the seed point and the posterior cortical regions. This is due to the generally high anisotropy observed in this region, leading to low uncertainty in fibre direction.

Figure 7 shows patterns of connection to a region placed in the left superior longitudinal fasciculus. The end points of the measured tract terminate in Broca's area and Wernicke's area. However, it is also evident that probability of connection is assigned to pathways that approach motor regions. Non-zero probability is also assigned to a region in the parietal lobe. These connections are unlikely to be present in the underlying anatomy.

Figure 8 demonstrates probabilities of connection to a single point in the left pyramidal body. The corticospinal tract connected to this point is well-defined throughout, indicating low uncertainty in fibre direction along its length.

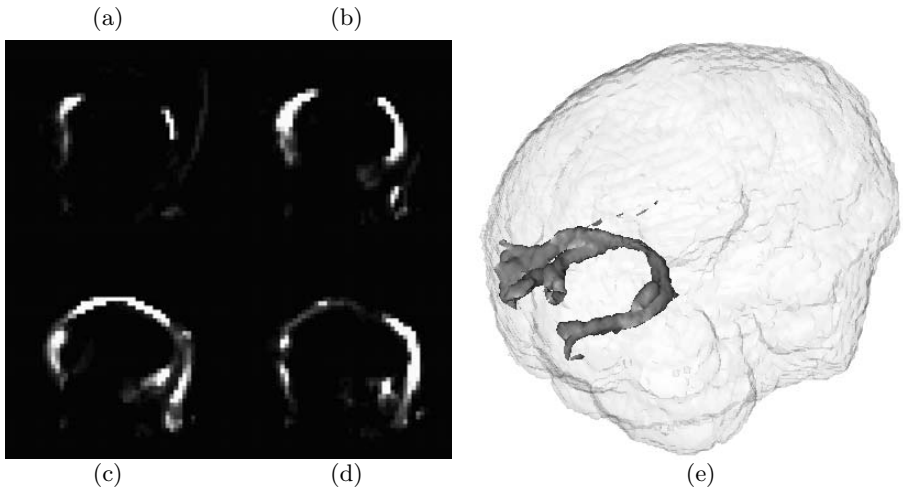


Fig. 6. Maps of connection probability to a seed point placed in the centre of the splenium of the corpus callosum. (a)–(d) adjacent slices of increasingly superior anatomical location. Radiological viewing convention used. Greyscale windowed to show full range of connection probability. (e) surface rendering showing thresholded probability values in corpus callosum. Note branching of identified connected regions in left hemisphere but an otherwise tightly localised pattern of connection

4 Discussion

We have identified voxels within the brain that include more than one fibre orientation and, by modelling the effects of noise, obtained PDFs on the PDDs for both the single and dual fibre cases. These PDFs are characterised as independent normal distributions in the angle of deflection away from the initial estimate of the PDD. The standard deviation of these distributions is shown to be related simply to the anisotropy of the tensors used in the model.

Using the crossing fibre information and the orientation PDFs we have shown that it is possible to generate probabilistic representations of diffusion-based voxel-scale connectivity from user-defined start points. This mapping benefits from the increased information content provided by the multi-tensor decomposition, which allows more accurate definition of the routes and termini of connections. It is also possible to use these data for deterministic fibre tracking (for example streamline methods (Fig. 5(a))), which again benefits from the improved information content. We have presented results in a single brain; results from a group of 10 further brains showed compatible results (not shown).

Validation of the method is to date limited to cross-referencing the results with known anatomy. This is undesirable, as knowledge of anatomy may be incomplete, and quantification of errors is difficult. Improved validation may be achieved with the use of data simulations and via the use of animal models. Also, the repeatability of the method could be assessed by repeated data ac-

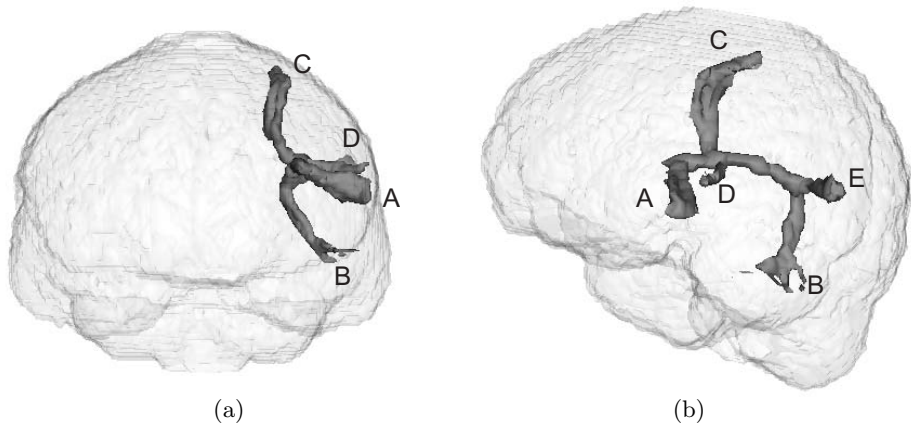


Fig. 7. Views of thresholded probability map in the left superior longitudinal fasciculus with rendered brain surface. Probability of connection to seed region in superior longitudinal fasciculus shows evidence of connection to Broca's area (A), Wernicke's area (B), motor areas (C, D), and an unidentified parietal/occipital region (E). (a) frontal view; (b) view from left

quisitions in a single subject. Notwithstanding the limitations on validation, the connections identified may be categorised as likely true positive and false positive in terms of the likely underlying anatomy. For example, the linkage between Broca's area and Wernicke's area demonstrated in Fig. 7 is as expected from known functional neuroanatomy. However, the connections, from the same start point, to motor regions in Fig. 7 are not expected. The fact that it is not possible to distinguish these two sets of connections as more or less likely from the data alone identifies a fundamental limitation of diffusion imaging-based fibre tracking. The uncertainties that we are able to define in one or more underlying fibre bundles reflect the fact that diffusion imaging gives us an imprecise indication of these orientations, which does not allow us to define connections unambiguously. Given the data, these regions are roughly equally likely to be connected to our start point; given known anatomy some of these are unlikely. In light of such observations it seems that relating diffusion imaging based findings to anatomy will always require significant expert knowledge, interpretation, and guidance (for example via the use of constraining volumes of interest [4]). Possible relaxation on these restrictions could be achieved by a reduction in data noise or a reduction in the sensitivity of the parameterisation process to noise, leading to a decrease in the variance seen in Figs 2 and 4. This would reduce the amount of dispersion in the connection probability maps and possibly reduce the occurrence of erroneous connections.

Another possibility for reducing 'false positive' connections is the introduction of constraints on the tracking process, such as curvature penalties, or regularisation of the diffusion data. However, curvature restrictions penalise genuine pathways demonstrating high curvature (for example the optic radiation), and

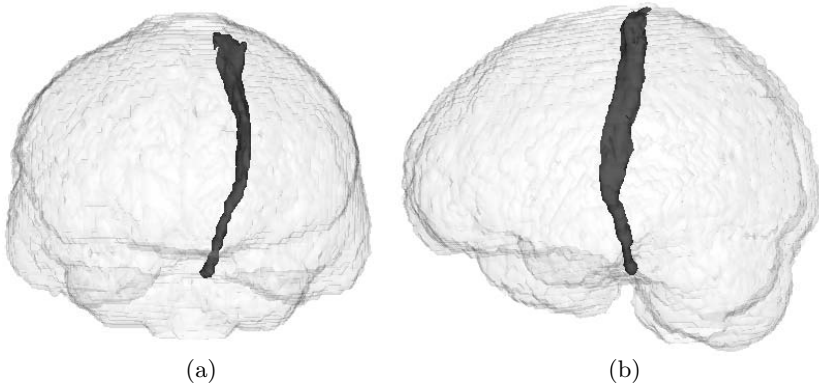


Fig. 8. Views of thresholded probability map of connections to the left pyramidal body with rendered brain surface. (a) frontal view; (b) view from left

regularisation methodologies may destroy potentially useful information and often also require curvature penalties. It may also be possible to extend the design of the PDFs to allow fibre orientation information from the local neighbourhood to be included, thus improving the focus of the PDF. However, without such advances in data interpretation and/or improvements in data quality, care must be employed when interpreting the results of diffusion connectivity studies.

Acknowledgements. We are grateful to Dr Olga Ciccarelli and Dr Claudia Wheeler-Kingshott, Institute of Neurology, London, for acquiring and making the data available. We also thank Dr Simona Luzzi, University of Manchester, for assistance with identification of neuroanatomical regions. This work has been supported in part by the Medical Research Council and the Engineering and Physical Sciences Research Council of Great Britain Interdisciplinary Research Collaboration “From Medical Images and Signals to Clinical Information,” under Grant GR/N14248/01.

References

1. Alexander, A.L., Hasan, K.M., Mariana, L., Tsuruda, J.S., Parker, D.L.: Analysis of partial volume effects in diffusion-tensor MRI. *Magn. Reson. Med.* **45** (2001) 770–780
2. Alexander, D.C., Barker, G.J., Arridge, S.R.: Detection and modelling of non-Gaussian apparent diffusion coefficient profiles in human brain data. *Magn. Reson. Med.* **48** 2002 331–340
3. Behrens, T.E.J., Jenkinson, M., Brady, J.M., Smith, S.M.: A probabilistic framework for estimating neural connectivity from diffusion weighted MRI. *Proc. Int. Soc. Magn. Reson. Med.* (2002) 1142

4. Conturo, T.E., Lori, N.F., Cull, T.S., Akbudak, E., Snyder, A.Z., Shimony, J.S., McKinstry, R.C., Burton, H., Raichle, M.E.: Tracking neuronal fiber pathways in the living human brain. *Proc. Nat. Acad. Sci. USA* **96** (1999) 10422–10427
5. Frank, L.R.: Characterization of anisotropy in high angular resolution diffusion-weighted MRI. *Magn. Reson. Med.* **47** (2002) 1083–1099
6. Jones, D.K., Horsfield, M.A., Simmons, A.: Optimal strategies for measuring diffusion in anisotropic systems by magnetic resonance imaging. *Magn. Reson. Med.* **42** (1999) 515–525
7. Jones, D.K.: Determining and visualizing uncertainty in estimates of fiber orientation from diffusion tensor MRI. *Magn. Reson. Med.* **49** (2003) 7–12
8. Koch, M.A., Norris, D.G., Hund-Georgiadis, M.: An investigation of functional and anatomical connectivity using magnetic resonance imaging. *NeuroImage* **16** (2002) 241–250
9. Lazar, M., Alexander, A.L.: White matter tractography using random vector (RAVE) perturbation. *Proc. Int. Soc. Magn. Reson. Med.* (2002) 539
10. Parker, G.J.M., Barker, G.J., Buckley, D.L.: A probabilistic index of connectivity (PICo) determined using a Monte Carlo approach to streamlines. *ISMRM Workshop on Diffusion MRI (Biophysical Issues)*, Saint-Malo, France (2002) 245–255
11. Parker, G.J.M., Barker, G.J., Thacker, N.A., Jackson, A.: A framework for a streamline-based probabilistic index of connectivity (PICo) using a structural interpretation of anisotropic diffusion. *Proc. Int. Soc. Magn. Reson. Med.* (2002) 1165
12. Pierpaoli, C., Basser, P.J.: Toward a quantitative assessment of diffusion anisotropy. *Magn. Reson. Med.* **36** (1996) 893–906
13. Stejskal, E.O., Tanner, J.E.: Spin diffusion measurements: spin echoes in the presence of a time-dependent field gradient. *J Chem Phys* **42** (1965) 288–292
14. Symms, M.R., Barker, G.J., Franconi, F., Clark, C.A.: Correction of eddy-current distortions in diffusion-weighted echo-planar images with a two-dimensional registration technique. *Proc. Int. Soc. Magn. Reson. Med.* (1997) 1723
15. Tuch, D. S., Wiegell, M. R., Reese, T. G., Belliveau, J. W., and Weeden, V. J. Measuring cortico-cortical connectivity matrices with diffusion spectrum imaging. *Proc. Int. Soc. Magn. Reson. Med.* (2001) 502
16. Wheeler-Kingshott, C.A.M., Boulby, P.A., Symms, M.R., Barker, G.J.: Optimised cardiac gating for high angular-resolution whole-brain DTI on a standard scanner. *Proc. Int. Soc. Magn. Reson. Med.* (2002) 1118